

 Open access • Journal Article • DOI:10.1039/C7EM00232G

## Minor methane emissions from an Alpine hydropower reservoir based on monitoring of diel and seasonal variability — [Source link](#)

Sébastien Sollberger, Sébastien Sollberger, Bernhard Wehrli, Bernhard Wehrli ...+4 more authors

**Institutions:** ETH Zurich, Swiss Federal Institute of Aquatic Science and Technology

**Published on:** 18 Oct 2017 - Environmental Science: Processes & Impacts (The Royal Society of Chemistry)

**Topics:** Eddy covariance and Surface water

Related papers:


- [Environmental controls on methane fluxes in a cool temperate bog](#)
- [CO<sub>2</sub> is Dominant Greenhouse Gas Emitted from Six Hydropower Reservoirs in Southeastern United States during Peak Summer Emissions](#)
- [High Methane Emissions from a Midlatitude Reservoir Draining an Agricultural Watershed](#)
- [Contrasting methane emissions from upstream and downstream rivers and their associated subtropical reservoir in eastern China.](#)
- [Spatial and temporal variability of urban fluxes of methane, carbon monoxide and carbon dioxide above London, UK](#)

Share this paper:    

View more about this paper here: <https://typeset.io/papers/minor-methane-emissions-from-an-alpine-hydropower-reservoir-11g5v0zem3>

# Minor methane emissions from an Alpine hydropower reservoir based on monitoring of diel and seasonal variability

**Journal Article****Author(s):**

Sollberger, Sébastien; Wehrli, Bernhard; Schubert, Carsten J.; DelSontro, Tonya; [Eugster, Werner](#) 

**Publication date:**

2017-10

**Permanent link:**

<https://doi.org/10.3929/ethz-b-000218541>

**Rights / license:**

[In Copyright - Non-Commercial Use Permitted](#)

**Originally published in:**

Environmental Science: Processes & Impacts 19(10), <https://doi.org/10.1039/c7em00232g>

Cite this: DOI: 10.1039/xxxxxxxxxxx

## Minor methane emissions from an Alpine hydropower reservoir based on monitoring of diel and seasonal variability

Sébastien Sollberger,<sup>a,b</sup> Bernhard Wehrli,<sup>a,b</sup> Carsten J. Schubert,<sup>a</sup> Tonya DelSontro,<sup>a,b,c</sup> and Werner Eugster<sup>\*d</sup>

Received Date  
Accepted Date

DOI: 10.1039/xxxxxxxxxxx

www.rsc.org/journalname

We monitored CH<sub>4</sub> emissions during the ice-free period of an Alpine hydropower reservoir in the Swiss Alps, Lake Klöntal, to investigate mechanisms responsible for CH<sub>4</sub> variability and to estimate overall emissions to the atmosphere. A floating eddy-covariance platform yielded total CH<sub>4</sub> and CO<sub>2</sub> emission rates at high temporal resolution, while hydroacoustic surveys provided no indication of CH<sub>4</sub> ebullition. Higher CH<sub>4</sub> fluxes ( $2.9 \pm 0.1$  mg CH<sub>4</sub> m<sup>-2</sup> d<sup>-1</sup>) occurred during the day when surface water temperatures were warmer and wind speeds higher than at night. Piston velocity estimates ( $k_{600}$ ) showed an upper limit at high wind speeds that may be more generally valid also for other lakes and reservoirs with limited CH<sub>4</sub> dissolved in the water body: above 2.0 m s<sup>-1</sup> a further increase in wind speed did not lead to higher CH<sub>4</sub> fluxes, because under such conditions it is not the turbulent mixing and transport that limits effluxes, but the resupply of CH<sub>4</sub> to the lake surface. Increasing CH<sub>4</sub> fluxes during the warm season showed a clear spatial gradient once the reservoir started to fill up and flood additional surface area. The warm period contributed 27% of the total CH<sub>4</sub> emissions (2.6 t CH<sub>4</sub> yr<sup>-1</sup>) estimated for the full year and CH<sub>4</sub> accounted for 63% of carbonic greenhouse gas emissions. Overall, the average CH<sub>4</sub> emissions (1.7 to 2.2 mg CH<sub>4</sub> m<sup>-2</sup> d<sup>-1</sup> determined independently from surface water samplings and eddy covariance, respectively) were small compared to most tropical and some temperate reservoirs. The resulting greenhouse gas (GHG) emissions in CO<sub>2</sub>-equivalents revealed that electricity produced in the Lake Klöntal power plant was relatively climate-friendly with a low GHG-to-power output ratio of 1.24 kg CO<sub>2,eq</sub> MWh<sup>-1</sup> compared to 6.5 and 8.1 kg CO<sub>2,eq</sub> MWh<sup>-1</sup> associated with the operation of solar photovoltaics and wind energy, respectively, or about 980 kg CO<sub>2,eq</sub> MWh<sup>-1</sup> for coal-fired power plants.

### Environmental Impact

Hydropower plants provide renewable energy, but their carbon footprint depends on their greenhouse gas emissions. In this case study of an Alpine storage reservoir, we focus on the pathways of CH<sub>4</sub> emissions, their spatial gradients and their variability over diel and seasonal cycles. Observations during 13 months reveal that CH<sub>4</sub> and CO<sub>2</sub> emissions are restricted to diffusive pathways. The lack of an emission pathway via gas bubbles is one factor why specific emissions of CO<sub>2</sub> equivalents per megawatt-hour are almost three orders of magnitude smaller than for typical coal-fired power plants. This high resolution study confirms earlier surveys that estimated smaller carbon footprints for Alpine storage reservoirs compared to run-of-the river plants in the lowlands.

<sup>a</sup> Eawag, Swiss Federal Institute of Aquatic Science and Technology, Department of Surface Waters, CH-6047 Kastanienbaum, Switzerland.

<sup>b</sup> Institute of Biogeochemistry and Pollutant Dynamics, Department of Environmental Systems Science, ETH Zürich, CH-8092 Zürich, Switzerland

<sup>c</sup> Current address: Department of Biological Sciences, University of Québec in Montréal, 8888 Montréal, Canada. E-mail: tdelontro@gmail.com

<sup>d</sup> Institute of Agricultural Sciences, Department of Environmental Systems Science, ETH Zürich, CH-8092 Zürich, Switzerland. E-mail: eugsterw@ethz.ch

\* Corresponding author.

# 1 Introduction

Hydropower plants are important sources of renewable energy and they are often considered “green energy”<sup>1</sup>. However, over the last two decades, studies have shown that reservoirs can be significant greenhouse gas (GHG) emitters<sup>2</sup>. Recent studies estimated the GHG strength of methane (CH<sub>4</sub>) and carbon dioxide (CO<sub>2</sub>) emissions from reservoirs globally as 0.5–1.2 Pg CO<sub>2,eq</sub> yr<sup>-1</sup><sup>3</sup>. A recent global synthesis of reservoir emissions suggests that CH<sub>4</sub> contributes up to 80% of the total radiative forcing by reservoirs<sup>3</sup>. The primary reason that CH<sub>4</sub> dominates the radiative forcing of reservoirs and other aquatic sources is linked to the fact that the global warming potential (GWP) of CH<sub>4</sub> is 34 times larger than that of CO<sub>2</sub>, on a 100 year time-scale, including positive climatic feedbacks<sup>4</sup>. In addition, the low solubility of CH<sub>4</sub> in water favors the direct transfer to the atmosphere via bubbles<sup>5,6</sup>. In contrast to slower emissions via diffusion, this ebullitive pathway bypasses the effective methane oxidation by bacteria that can substantially limit atmospheric emissions<sup>7–9</sup>. Importantly, when ebullitive emissions are included in more comprehensive estimates of inland water carbon emissions, it appears that aquatic carbon emissions may partially offset the global continental carbon sink<sup>10</sup>. Ultimately, improving our mechanistic understanding of CH<sub>4</sub> emissions from different types of water bodies has been identified as an important research priority, particularly for man-made hydroelectric reservoirs<sup>10,11</sup> given that global hydropower capacity is estimated to increase by 73% over the coming decades<sup>12</sup>.

A large uncertainty in global CH<sub>4</sub> emission estimates from reservoirs is partially linked to the lack of detailed emission studies, particularly ones with rigorous analysis of the contributions by both ebullitive and diffusive pathways which requires detailed considerations of temporal and spatial coverage of total emissions depending on methodology<sup>3</sup>. Such data gaps were mostly due to the methods chosen for gas emission surveys, which were typically floating chambers and gas traps that merely report point measurements of gas flux<sup>13–15</sup>. Fortunately, several measurement techniques are now available to help better constrain the role of reservoirs as global CH<sub>4</sub> sources. Hydroacoustic techniques via an echosounder can easily detect the presence or absence of bubble plumes as well as quantify ebullitive emissions following certain calibration procedures<sup>6,16–18</sup>. The eddy-covariance (EC) technique is best suited to monitor seasonal cycles and short-term changes of total surface CH<sub>4</sub> emissions<sup>19–24</sup>. These methods, however, remain costly and, thus, most surveys are still performed with low cost alternative methods such as floating chambers<sup>14</sup>, air–water exchange calculations using measured dissolved gas concentrations and wind speed<sup>25</sup>, and depth profiles for gas budgets that include storage or turnover emissions<sup>13,26</sup>.

Therefore, here, we combine several different gas emission observation techniques, including high resolution ones, in order to constrain and present a comprehensive and annual CH<sub>4</sub> emission budget for Lake Klöntal, a medium-sized 60 MW hydropower scheme in the Swiss Alps. An EC flux tower was deployed throughout the ice-free season to evaluate diel and seasonal changes in CH<sub>4</sub> and CO<sub>2</sub> emissions, which was compli-

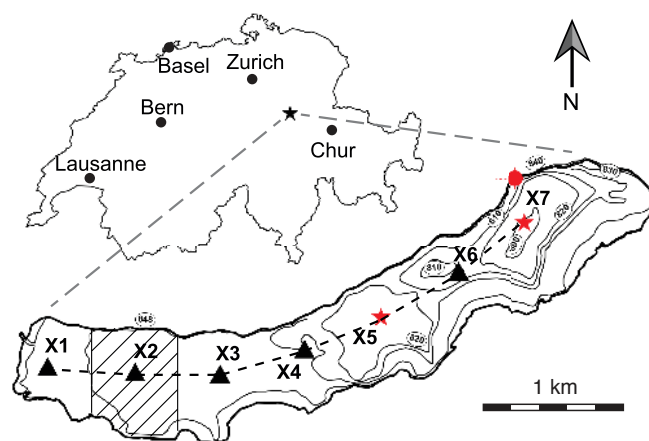


**Fig. 1** Location of Lake Klöntal and sampling locations. Symbols show the surface (triangles) and profile (stars) sampling locations, while the circle shows the location of the EC system close to the dam outlet. The shaded area is an example, how CH<sub>4</sub> emissions measured at X2 were weighed for lake total efflux estimates.

mented by surface sampling along the reservoir to assess how representative the EC flux measurements were for the entire reservoir. In addition, hydroacoustic surveys for CH<sub>4</sub> ebullition were conducted. Combining these spatial and temporal observations, we calculate the specific emission rate of this Alpine storage reservoir to approximate the carbon footprint in kg CO<sub>2,eq</sub> MWh<sup>-1</sup> of this high-mountain hydropower reservoir.

## 2 Material and methods

### 2.1 Study sites

Lake Klöntal is a hydropower reservoir located in the northern Swiss Alps (47°01'32"N, 8°58'50"E, Fig. 1) that has a maximum water depth of 45 m, a volume of 39.8·10<sup>6</sup> m<sup>3</sup> and a maximum water level of 847 m a.s.l. It is surrounded by two high mountain ranges (> 2000 m a.s.l.) running from east to west. The climate (Fig. 2) is cold temperate with a mean annual temperature (MAT) of 10.9 and 9.4°C in 2011 and 2012, respectively. Absolute minimum (maximum) temperatures were –9.6 and –18.1°C (30.5 and 30.6°C). Annual precipitation was 2125 mm in 2011 and 2600 mm in 2012, of which 40% and 58% was snowfall in 2011 and 2012, respectively. A rain gauge of the Swiss national weather service MeteoSwiss with hourly-resolving data collection was only installed in 2013. From this site located at the west end of Lake Klöntal we used precipitation intensity data from 29 August 2013 until 31 December 2016 at hourly resolution. During this period, 86.3% was rainfree, 90% of the time precipitation intensity was ≤0.4 mm h<sup>-1</sup>, 95% ≤1 mm h<sup>-1</sup>, 99% ≤7.8 mm h<sup>-1</sup>, and the maximum was 34.8 mm h<sup>-1</sup>.

The Klöntal hydropower plant (Fig. 1) was finished in 1908 and produces on average 114 GWh of electricity annually. The reservoir surface varies between 1.2 km<sup>2</sup> (minimum water level, 829 m a.s.l.) and 3.3 km<sup>2</sup> (maximum water level, 847 m a.s.l.) and is covered by snow and ice during three months of the year (mid-December until mid-March). After snowmelt, the water level generally rises by ca. 15 m from May through July. During this pe-

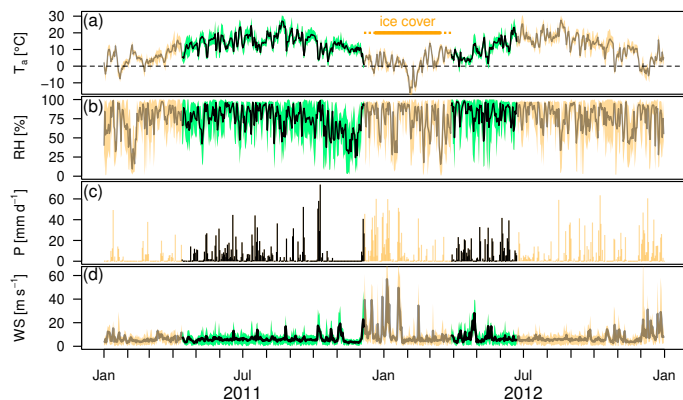


**Fig. 2** Meteorological conditions in years 2011 and 2012, (a) air temperature; (b) relative humidity; (c) daily precipitation; (d) wind speed at 10 m above ground. The periods with EC flux measurements on the lake are plotted with green color and bold lines, and the periods not covered by this study are shown with orange color and opaque lines. Data retrieved from Meteoblue.com.

riod, the surface area of the reservoir almost doubles and then decreases again in winter.

## 2.2 CH<sub>4</sub> and CO<sub>2</sub> flux monitoring using the eddy covariance technique

During the ice-free period from April until December 2011 and from March until June 2012, we continuously measured the CH<sub>4</sub> flux using an EC system. The EC system consisted of an FMA-100 fast CH<sub>4</sub> analyzer (Los Gatos Research Inc., Mountain View, CA, USA) and a Solent R2A ultrasonic anemometer (Gill Instruments Ltd., Lymington, UK) as described in detail by Eugster and Plüss<sup>27</sup>. The sensor head was placed 1.49 m above the water surface on a floating aluminum frame in 2011 (1.72 m in 2012). The analyzer was protected by a water trap to prevent dust, moisture and droplets from penetrating the sample cell. The analyzer and gas inlet were moored on a skeleton raft roughly 50 m off the shore of the reservoir, almost identical to an earlier deployment at Rotsee<sup>20</sup>. A high-performance vacuum pump was used for carrying gas through an 8 mm inner diameter Synflex-1300 hose (Eaton Performance Plastics, Cleveland, OH, USA) to the analyzer on shore, and raw data were recorded at 20.8 Hz<sup>27</sup>. This allowed us to measure fluxes at high frequency for further analysis of the diel and seasonal variability. The platform was removed for winter before ice-on, but replaced again by the end of March 2012 to continue the experiment for an additional three months.

In 2012, additional water vapor and CO<sub>2</sub> flux measurements were performed with an infra-red gas analyser (Li-Cor 7500, Lincoln, NE, USA) since CH<sub>4</sub> fluxes were surprisingly low compared to earlier deployments elsewhere<sup>19,20</sup> and thus a flux correction for density fluctuations associated with water vapor fluctuations was needed<sup>28</sup>. The closed-path FMA-100 measured CH<sub>4</sub> concentrations with respect to moist air, not dry air, and hence density fluctuations caused by concurrent water vapor fluctuations may bias CH<sub>4</sub> flux measurements<sup>28</sup>. Since no such additional measurements were available in 2011, the density flux correction in 2011 was approximated by an empirical relationship obtained

from 2012 flux data. For this, a stepwise elimination multiple regression approach was used in which all time series variables that were also measured in 2011 were used as candidate predictor variables for the density fluctuation correction term (*DFC*). In each step the variables with insignificant explanatory power (t-test yielded  $p > 0.05$ ) were eliminated. The final model for *DFC* was

$$DFC \approx \alpha_1 \cdot \sqrt{w^2} + \alpha_2 \cdot \overline{w^2} + \alpha_3 \cdot \sqrt{m^2} + \alpha_4 \cdot H, \quad (1)$$

where  $w^2$  and  $m^2$  are the variance of the vertical and horizontal (scalar) wind velocity components ( $\text{m}^2 \text{s}^{-2}$ ), and  $H$  is a cyclical hour variable derived from hour of day CET (hh) as  $H = |\text{hh} - 13|$ . Overbars denote averaging over standard 30-minute periods, and  $\alpha_1$ – $\alpha_4$  are regression coefficients determined via least-squares fitting. Adjusted  $r^2$  was 0.637 ( $p < 0.0001$ ) with  $\alpha_1 = (1.62 \pm 0.07) \cdot 10^{-10}$ ,  $\alpha_2 = (-1.54 \pm 0.08) \cdot 10^{-10}$ ,  $\alpha_3 = (6.4 \pm 1.7) \cdot 10^{-12}$ , and  $\alpha_4 = (-6.7 \pm 0.7) \cdot 10^{-13}$ . The empirically determined *DFC* has units of  $\text{kg CH}_4 \text{ m}^{-2} \text{ s}^{-1}$  and was added to the measured CH<sub>4</sub> flux. These additional measurements in 2012 also provided CO<sub>2</sub> fluxes, which were corrected for density fluctuations by both sensible and latent heat fluxes in the standard way described by Webb et al.<sup>28</sup>.

The data collection and processing closely followed the recommendations for EC flux measurements over lakes<sup>21</sup> using our in-house eth-flux software<sup>29</sup>. Unrealistic spikes in raw data were filtered out, and the quality of the remaining fluxes was assessed using Foken's quality flags<sup>30</sup> for steady-state conditions during each 30-minute averaging interval. Fluxes did not require a special correction for the oscillation of the platform as was shown in detail by Eugster et al.<sup>31</sup>. During the two measurement periods in 2011 and 2012 the data coverage was 89.9% with 6334 hours of valid data. Of these 83.7% can be considered of good or best quality (with 26.4% best quality) and 16.3% of poor quality that are useful for monthly and annual averages but not good enough for in-depth investigations of half-hour intervals. The flux footprint analysis with the Kljun model<sup>32</sup> shows that the flux footprint in all wind directions almost perfectly covers lake surface and is not affected directly by the surrounding terrain (Fig. 3).

## 2.3 Hydroacoustical determination of ebullition

Ebullition surveys were conducted during two campaigns in July and September 2011, two months of warmest weather in which ebullition would occur if at all. We used a split-beam echosounder (Simrad EK60, 7° beam angle) with a 120 kHz transducer pinging at 5 Hz, as described by DelSontro et al.<sup>6</sup>, along a grid of 50×50 m throughout the reservoir surface.

## 2.4 Spatial explicit water sampling and flux estimates

From April–December 2011 water samples were taken monthly at two locations (X5 & X7, Fig. 1). As the first samplings in April 2011 showed substantial differences in surface water concentrations at X5 and X7, additional measurements (X1–4 and X6, Fig. 1) were carried out starting in August 2011 so that a sample was taken about every 500 m along the reservoir. Water was col-

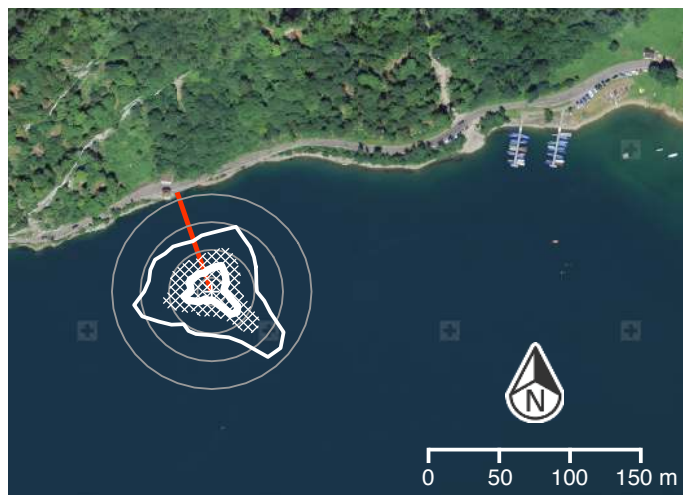


**Fig. 3** Flux footprint area covered by the eddy covariance system. Bold line: median of wind direction-specific footprint area; outer thick line: 90% extent of the footprint area; hashed area: 50% of the direction specific footprint area. Red line: intake hose and electrical cables connecting sensors on floating platform with analyser and data acquisition in the building on shore. Gray circles around the eddy covariance system are drawn at 30, 50 and 70 m distance for reference. Background image © swisstopo, reprint permission JD100042.

lected in 120 ml glass vials and poisoned with CuCl to prevent microbial activity. The samples were sealed bubble-free using butyl stoppers and aluminum caps. Gas samples were analyzed for CH<sub>4</sub> concentrations by gas chromatography (Agilent 6890 gas chromatograph equipped with a flame ionization detector (FID), Agilent Technologies Inc., Santa Clara, USA). Conductivity-temperature-depth (CTD) casts and vertical CH<sub>4</sub> profiles were conducted at locations X5 and X7 down to maximum summer depths of 30 and 45 m, respectively.

Dissolved CH<sub>4</sub> concentration measurements in surface waters carried out between April and November 2011 at location X7 were used in combination with EC flux measurements during the same time period to estimate a piston or gas exchange velocity ( $k$ ) that could be used to estimate CH<sub>4</sub> flux at other locations on the reservoir where the EC footprint (Fig. 3) could not account for but surface concentrations were taken (i.e., locations X1–X6). The governing flux equation is<sup>33</sup>

$$F_{CH_4} = k_{CH_4} \cdot (C_w - C_{eq}), \quad (2)$$

where CH<sub>4</sub> flux,  $F_{CH_4}$  (mg CH<sub>4</sub> m<sup>-2</sup> d<sup>-1</sup>) is the product of the piston velocity,  $k_{CH_4}$  (cm h<sup>-1</sup> or m d<sup>-1</sup>), and the CH<sub>4</sub> concentration gradient across the air–water interface that is equal to the difference between dissolved CH<sub>4</sub> in the water,  $C_w$  (nM), and surface water in equilibrium with atmospheric CH<sub>4</sub> concentrations,  $C_{eq}$  (nM).  $C_w$  was found as described above and measurements at location X7 were used because it was directly upwind of the eddy covariance flux system during typical daytime conditions with winds from the southeast (Fig. 4a).  $C_{eq}$  was calculated according to Wiesenburg and Guinasso<sup>34</sup> using an atmospheric CH<sub>4</sub> concentration of 1.803 ppm<sup>35</sup>.

We used five different published models proposed for  $k_{600}$ , the

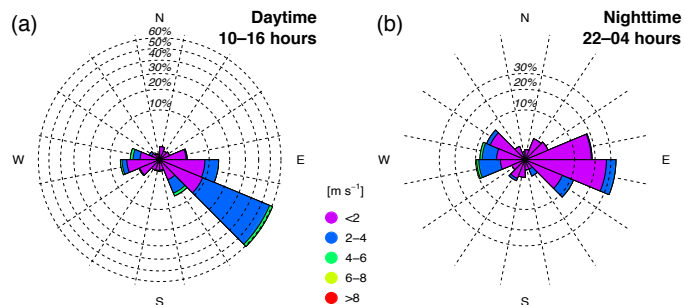


**Fig. 4** Windroses observed by the EC system during (a) daytime and (b) nighttime. The dominant southeasterly direction is typically associated with slightly higher wind speeds (>2 m s<sup>-1</sup>) than those observed from other directions. Calm conditions with wind speeds <1 m s<sup>-1</sup> were excluded.

piston velocity normalized to a Schmidt number of 600 (Table 1, models 1–5), to determine the CH<sub>4</sub> flux with equation (2) and

$$k_{CH_4} = k_{600} \left( \frac{600}{Sc_{CH_4}} \right)^{-n}. \quad (3)$$

$k_{600}$  is parametrized for constant oversaturation at the water–air interface at variable wind speeds. This condition is usually met in oceans, where most of these parametrizations have been done, because of intense surface mixing and rather limited gradients of dissolved gas. In the Klöntal case the difference between the five models was very large, and thus the average  $k_{600}$  from all five models was used for the spatial integration, thereby keeping this estimate independent of the EC flux measurements.

## 2.5 Validation of piston velocity

For validation of this approach, we however also back-calculated  $k_{600}$  using EC fluxes and concentration measurements in the water interpolated over time (see below). In this way, equation (2) was solved for  $k_{CH_4}$ , which then was normalized to a  $k$  for CO<sub>2</sub> at 20°C in freshwater ( $k_{600}$ ) using the following equation<sup>33,41</sup>,

$$k_{600} = k_{CH_4} \left( \frac{600}{Sc_{CH_4}} \right)^n, \quad (4)$$

where  $Sc_{CH_4}$  is the Schmidt number for CH<sub>4</sub>, which was calculated here according to Wanninkhof<sup>42</sup>, and  $n$  is a constant that depends on the roughness of the water surface, which was set to  $-2/3$  when wind speeds were below 3.7 m s<sup>-1</sup> and set to  $-1/2$  when wind speeds were above 3.7 m s<sup>-1</sup><sup>43</sup>. As we had the ability for continuous flux measurements via the EC system,  $C_w$  and  $Sc_{CH_4}$  were estimated from measured surface concentrations at location X7 for each 30-min averaging interval using a local polynomial regression fit (loess function<sup>44</sup>) of second order with a span of 0.7 for both  $C_w$  and water temperature  $T_w$ , from which  $Sc_{CH_4}$  was calculated with

$$Sc_{CH_4} = 1897.8 - 114.28 T_w + 3.2902 T_w^2 - 0.039061 T_w^3. \quad (5)$$

As most  $k_{600}$  models are expressed according to wind speed at 10 m height,  $U_{10}$ , we converted EC wind speed (measured at

**Table 1** Empirical relationships between wind ( $U_{10}$ ) and piston velocity ( $k_{600}$ ) based on a threshold depending on either  $U_{10}$  or buoyancy flux ( $\beta$ ). Models 1–5 were averaged to compute spatially averaged fluxes, and model 6 was derived from eddy covariance flux data on Lake Klöntal for comparison.

Nr.	$k_{600}$ [cm h <sup>-1</sup> ]	Condition	Source
1.	$0.215U_{10}^{1.7} + 2.07$ $0.45U_{10}^{1.64}$	$U_{10} < 4.0$ m s <sup>-1</sup> $U_{10} \geq 4.0$ m s <sup>-1</sup>	Cole and Caraco (1998) <sup>36</sup>
2.	$0.72U_{10}$ $4.33U_{10} - 13.3$	$U_{10} < 3.7$ m s <sup>-1</sup> $U_{10} \geq 3.7$ m s <sup>-1</sup>	Crusius and Wanninkhof (2003) <sup>37</sup>
3.	$2.04U_{10} + 2.0$ $1.74U_{10} - 0.15$	$\beta > 0$ $\beta < 0$	MacIntyre et al. (2010) <sup>38</sup>
4.	$1.03 + 0.129U_{10}^2 + 19.99R_n$	$R_n =$ rainfall rate [cm h <sup>-1</sup> ]	Frost and Upstill-Goddard (2002) <sup>39</sup>
5. L	$(1.05 \pm 0.17)U_{10} + (0.74 \pm 0.67)$	bin averaged data	Guerin et al. (2007) <sup>40</sup> , linear model
5. P	$(1.76 \pm 0.77) + (0.23 \pm 0.32)U_{10}^{1.78 \pm 0.72}$	bin averaged data	Guerin et al. (2007) <sup>40</sup> , power model
5. E	$(1.66 \pm 0.34)e^{(0.26 \pm 0.04)U_{10}}$	bin averaged data	Guerin et al. (2007) <sup>40</sup> , exponential model
6.	$(0.25 \pm 0.08)U_{10}^{(4.92 \pm 0.49)} + (1.53 \pm 0.09)$ $9.12 \pm 0.37$	$U_{10} < 2.0$ m s <sup>-1</sup> $U_{10} \geq 2.0$ m s <sup>-1</sup>	This study

z=1.49 m and 1.72 m in 2011 and 2012, respectively) to  $U_{10}$  using the logarithmic wind profile,

$$U_{10} = U(z) + \frac{u_*}{k_a} \cdot (\ln 10 - \ln z) \quad (6)$$

## 2.6 Total annual CH<sub>4</sub> emission estimate

Finally, we integrated CH<sub>4</sub> flux derived at all locations to estimate total emissions from the lake (see Fig. 1). Each local flux measurement  $i$  was weighted by the surface area  $S_i$  of the lake section for which it was considered representative. Section boundaries were chosen mid-way between two sampling points as depicted for section X2 in Figure 1. Annual CH<sub>4</sub> emission  $E_{tot}$  (t yr<sup>-1</sup>) was estimated as follows:

$$E_{tot} = \alpha \sum_{j \in M_y} D_j \cdot \sum_{i \in X_m} F_{i,j} \cdot S_i \quad (7)$$

with  $M_y$  month of year  $y$  (2011, 2012),  $X_m$  sampling location X1–X7,  $D_j$  the number of days in month  $M_y$ , and  $F_{i,j}$  the CH<sub>4</sub> flux (in mg m<sup>-2</sup> d<sup>-1</sup>). The sum over all  $S_i$  corresponds to the maximum lake surface area (in m<sup>2</sup>), and  $\alpha = 10^{-9}$  t mg<sup>-1</sup> converts from mg CH<sub>4</sub> yr<sup>-1</sup> to t CH<sub>4</sub> yr<sup>-1</sup>. The sampling lasted for eight months during the ice-free period and reduced effluxes were assumed from December to March due to ice cover. Thus, the measured flux in April is expected to contain the signal of the CH<sub>4</sub> that may have accumulated under the ice during winter and is released to the atmosphere once the ice has disappeared. This spatial explicit approach was then compared with the EC fluxes measured near location X7, which provide a better temporal, but much lower spatial representativity.

## 3 Results

In order to disentangle diffusive and potential ebullitive pathways, we combined different surveys. The eddy covariance instrument allowed for an analysis of total diel emissions at one spot with a flux footprint area of  $\approx 100$  m<sup>2</sup>. The long observation period also provided a basis for quantifying the seasonal variability. The monthly surveys of surface CH<sub>4</sub> and its depth distribution allowed us to determine spatial gradients and the response of CH<sub>4</sub> emissions to water-level changes. Interestingly, ebullition

could be ruled out as a major emission pathway in Lake Klöntal. We conducted two hydroacoustic surveys during the warmest period and at maximum water level but we did not detect any CH<sub>4</sub> ebullition nor were any bubbles seen rising to the lake surface. This does not imply that ebullition never occurred in Lake Klöntal, but indicates that this process contributes little to the overall CH<sub>4</sub> emissions. The sonar surveys therefore indicated that the main emission pathway in this reservoir was via diffusion, and so the following analysis and discussion will focus on diffusive emissions.

### 3.1 Variations of gas concentrations in the water and the air

Diel variations in hourly median atmospheric CH<sub>4</sub> concentration (Fig. 5a) only varied between 1.875 and 1.891 ppm, thus only by  $\approx 1\%$ , with peak concentrations being synchronous with CH<sub>4</sub> effluxes (Fig. 5b). This indicates, that the increase in local atmospheric CH<sub>4</sub> concentrations is a result of the CH<sub>4</sub> losses from the lake, and hence the average CH<sub>4</sub> concentration was clearly above the global background of 1.803 ppm<sup>35</sup>.

Seasonal variations also remained in the narrow range from 1.774 to 2.225 ppm with the minimum and maximum concentration observed on 27 June and 7 November 2011, respectively (data not shown). Thus, on average, 2011 atmospheric CH<sub>4</sub> concentrations translated into a surface water equilibrium concentration of  $3.10 \pm 0.34$  nM (Fig. 6), which was  $\approx 2$  orders of magnitude less than 2011 observed surface water CH<sub>4</sub> concentrations and implied a constant outgassing of CH<sub>4</sub> from the reservoir surface.

CO<sub>2</sub> concentration measurements were only added in 2012 without parallel measurements of concentrations in the water since CO<sub>2</sub> effluxes were initially considered much less important than CH<sub>4</sub> effluxes. The daily averaged CO<sub>2</sub> concentrations ranged from 433 to 599 ppm (data not shown), which is clearly higher than the global average of 390.5 ppm in 2011<sup>35</sup>. The diel variations of hourly medians varied from 439 to 461 ppm (Fig. 5c), but were inversely related to CO<sub>2</sub> fluxes from the lake ( $r = -0.7027$  for hourly medians shown in Fig. 5d). This indicates that the lake most likely is only a weak source of CO<sub>2</sub> and that the diel CO<sub>2</sub> concentration variations are more affected by larger-scale emissions, atmospheric mixing, and plant uptake during daytime.

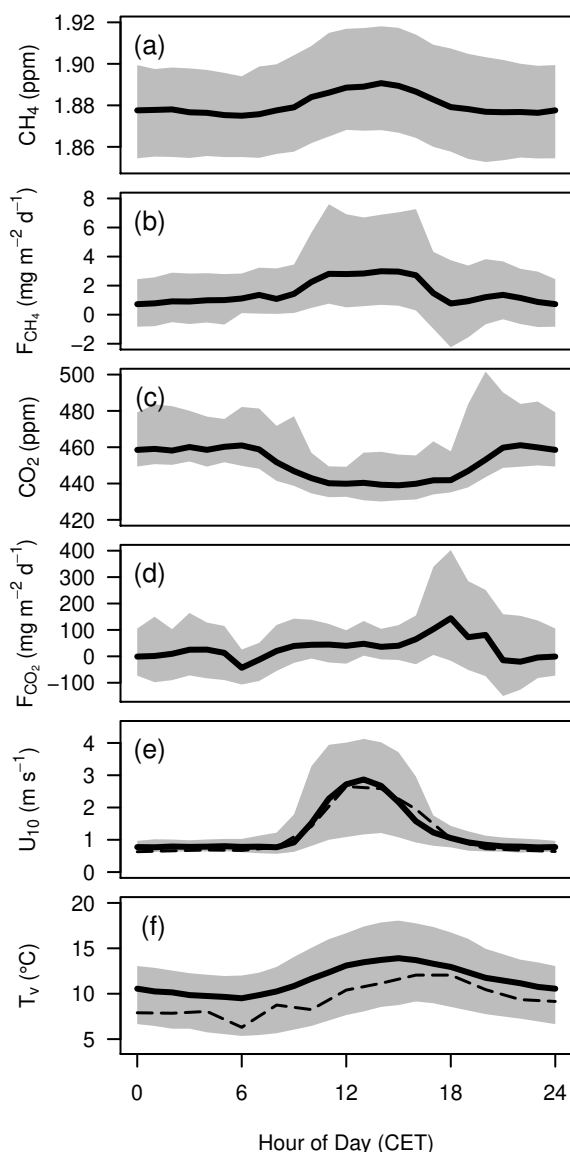


**Fig. 5** Hourly median (bold line) and inter-quartile range (gray band) of a) atmospheric CH<sub>4</sub> concentration (CH<sub>4</sub>), b) eddy covariance measured CH<sub>4</sub> flux ( $F_{CH_4}$ ), c) atmospheric CO<sub>2</sub> concentration (CO<sub>2</sub>), c) eddy covariance measured CO<sub>2</sub> flux ( $F_{CO_2}$ ), e) wind speed ( $U_{10}$ ), and f) virtual temperature ( $T_v$ ) measured between 13 April 2011 and 22 June 2012 (excluding months with ice cover before 13 April 2011 and between 6 December 2011 and 29 March 2012). The dashed lines in panels (e) and (f) show the hourly medians for the period with CO<sub>2</sub> concentration and flux measurements (29 March to 22 June 2012).

### 3.2 Validation of piston velocity estimation

The spatially averaged CH<sub>4</sub> fluxes computed from gas concentrations in the surface water (equation 2) strongly depend on the assumptions made for  $k_{CH_4}$  piston velocity, hence a validation with direct EC flux measurements as a function of wind speed was done. Figure 7 shows the result of 7.5 months of computed gas exchange coefficients, converted to  $k_{600}$  using equation (4), which was excellently correlated with  $U_{10}$ . To account for the non-uniform distribution of wind speeds, data were grouped in 50 wind speed classes with equal number of flux measurements (50 groups with  $N = 212$  half-hourly flux records each). For each

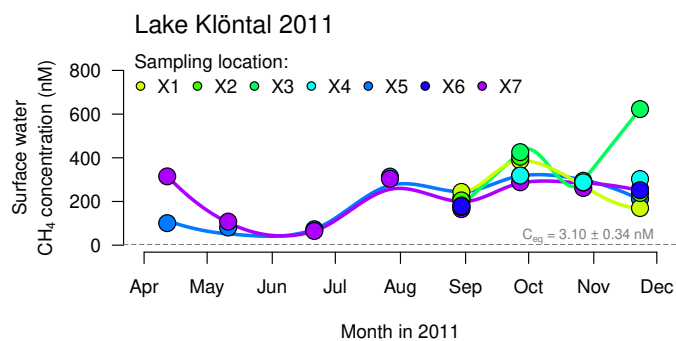


**Fig. 6** Seasonal evolution of surface water CH<sub>4</sub> concentrations in 2011 determined by the headspace equilibration method. At all times the water was supersaturated with CH<sub>4</sub> with respect to atmospheric concentration  $C_{eq}$  (gray horizontal dashed line).

group the median  $U_{10}$  and median  $k_{600}$  was calculated (circles in Fig. 7). A logistic curve fit well to these group medians. Note the logarithmic display of the  $U_{10}$  axis in Figure 7 to show the details at low wind speeds, which were dominant during the entire deployment of the system. The logistic approach has two important benefits for this application: (1) it has a lower and upper asymptote which agree much better with the empirical data than a simple exponential (or power law) or even a polynomial fit; and (2) in the central range of the logistic fit, the typical exponential increase of  $k_{600}$  with increasing  $U_{10}$  is still correctly reflected<sup>37</sup>. The best fit for  $k_{600}$  (in  $cm\ h^{-1}$ ) derived from EC-CH<sub>4</sub> flux measurements was

$$k_{600} = 2.1 + \frac{7.0 \pm 0.2}{1 + \exp\left(\frac{1.70 \pm 0.04 - U_{10}}{0.11 \pm 0.03}\right)}, \quad (8)$$

where the parameter estimates are given with their respective standard error of the best estimate. For practical applications, this equation was also approximated by a simplified approach with two  $U_{10}$  regimes given in Table 1 (model 6).

At low wind speeds  $< 1\ m\ s^{-1}$  the C1998 model<sup>36</sup> almost perfectly agrees with  $k_{600}$  calculated from our EC flux measurements, whereas most other models predicted lower  $k_{600}$ . Under conditions with positive buoyancy fluxes, the M2010 model<sup>38</sup> also predicted  $k_{600}$  correctly at wind speeds  $< 0.4\ m\ s^{-1}$ , but at  $U_{10}$  exceeding this threshold, M2010 leads to a substantial overestimation of  $k_{600}$ , unless the buoyancy flux is negative. The most important difference between published  $k_{600}$  models and measurements from Lake Klöntal, however, are (a) the narrow range of wind speeds ( $1\text{--}2\ m\ s^{-1}$ ) where  $k_{600}$  visibly increases in an exponential way similar to all other models, and (b) the upper limit of  $k_{600}$  at  $U_{10} > 2\ m\ s^{-1}$  when  $k_{600}$  remains constant at  $9.12 \pm 0.37\ cm\ h^{-1}$  irrespective of  $U_{10}$ .

### 3.3 Seasonal flux variations

The comparison of the methane profiles at the deepest site (X7) with the shallower location (X5) reveals rather low methane levels at the end of the winter season (black profiles in Fig. 8). In summer and autumn sediments at warm-water intermediate depths, 10–20 m, act as an important methane source and pro-



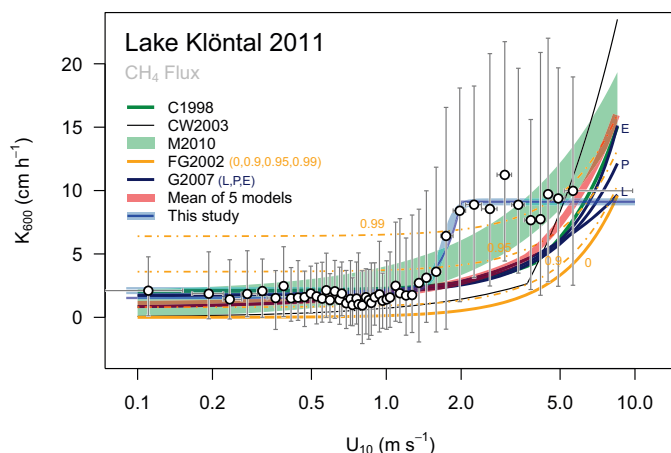


**Fig. 7** Piston velocity  $k_{600}$  determined from  $\text{CH}_4$  EC fluxes and air–water concentration gradients. 30-min averages were binned in 50 groups of equal number of samples. For each group the median (open circles) and the inter-quartile ranges (horizontal and vertical whiskers) are shown. A logistic fit was calculated for all median  $U_{10}$  values (bold blue curve), and a simplified power fit (thin blue line; see Table 1). Parametrizations used for the spatial flux estimations are shown for reference: C1998<sup>36</sup>, CW2003<sup>37</sup>, M2010<sup>38</sup>, FG2002<sup>39</sup>, and G2007<sup>40</sup>, and the mean of all five models (bold red curve), which uses FG2002 under absence of rainfall and the exponential version (E) of the G2007 model (L = linear; P = power). The dashed orange lines of the FG2002 model show the values for rainfall intensities that correspond to the 0.90, 0.95 and 0.99 percentiles measured at a nearby rainfall gauge. The broad band shown for M2010 shows the range depending on the buoyancy flux.

duce maxima in the profiles. The low concentrations in the deep waters indicate that the cold conditions at the lake bottom prohibit intense methane release from sediments.

The period until end of June 2011 was characterized by rising lake levels that filled the entire reservoir by early summer (Fig. 9b, blue line). While bottom water temperatures in the deep Eastern locations remained cold, the shallow inundation zone at the western locations warmed completely to the bottom (Fig. 9a). The rapid inflow of snowmelt enhanced the lake volume substantially, but the lake remained highly supersaturated with  $\text{CH}_4$  (Fig. 6). EC-derived  $\text{CH}_4$  fluxes aggregated at a monthly resolution (Fig. 10) follow the pattern of  $\text{CH}_4$  concentrations in surface waters (Fig. 6), except for November 2011 with the lowest median fluxes despite high  $\text{CH}_4$  supersaturation in the water due to exceptionally low wind speeds (Fig. 2). From mid-December 2011 until early March 2012, ice cover prevented EC deployment and, hence, flux measuring. For this period we assumed zero effluxes of  $\text{CH}_4$  and  $\text{CO}_2$ , assuming that the accumulated gas in the ice covered water will not evade until ice-out in spring. In March 2012, when the EC system could be again deployed on the lake, median fluxes were slightly higher compared to December 2011 before the onset of ice. This may be related to  $\text{CH}_4$  accumulating in the water under the ice cover, which is slowly emitted during and following ice melt. In contrast to 2011, the seasonal evolution of  $\text{CH}_4$  fluxes showed a pronounced decrease from  $4.6 \text{ mg CH}_4 \text{ m}^{-2} \text{ d}^{-1}$  in March 2012 to  $0.4 \text{ mg CH}_4 \text{ m}^{-2} \text{ d}^{-1}$  in June 2012 (monthly median values; Fig. 10 and Table 2). During the same

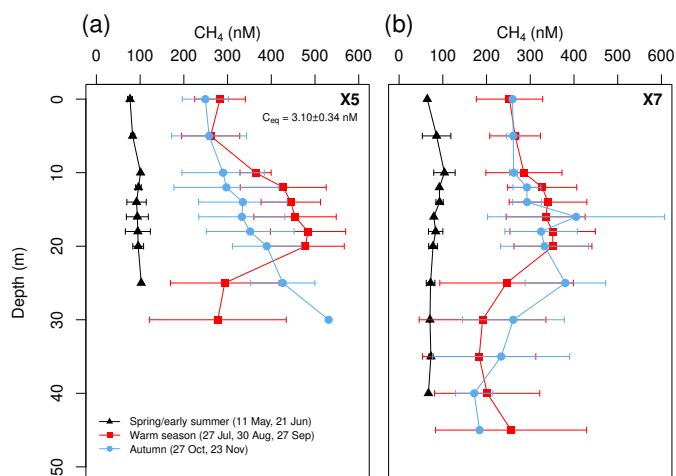


**Fig. 8** Mean  $\text{CH}_4$  concentration profiles (with standard deviation bars) at a) site X5 and b) site X7 in spring/early summer (11.05.2011; 21.06.2011), warm season (27.07.2011; 30.08.2011; 27.09.2011), and autumn (27.10.2011; 23.11.2011).  $C_{\text{eq}}$  is the mean ( $\pm$ SD)  $\text{CH}_4$  equilibrium concentration with the atmosphere for both sites using the atmospheric  $\text{CH}_4$  concentration measured at the eddy covariance flux site near X7.

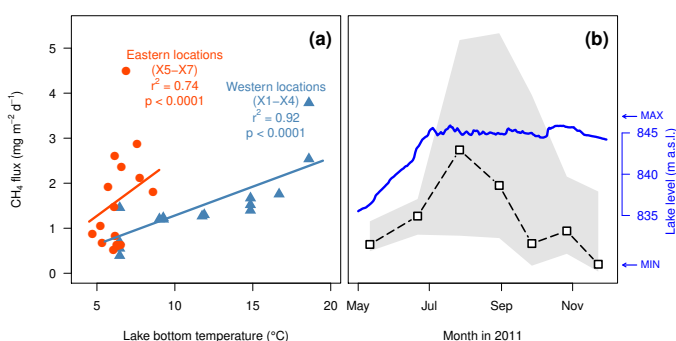


**Fig. 9** a) Relationship between lake bottom water temperatures and surface  $\text{CH}_4$  fluxes at the eastern (red line) and western (blue line) locations. b) Median seasonal variations of  $\text{CH}_4$  fluxes (squares) from water sampling at all seven locations using five different models to calculate  $k_{600}$ . Grey shaded area shows the inter-quartile range of all fluxes (left y-axis), and the blue line shows the water level (right y-axis).

months,  $\text{CO}_2$  fluxes exhibited an opposite trend starting with a net uptake of  $56 \text{ mg CO}_2 \text{ m}^{-2} \text{ d}^{-1}$  to a net efflux of  $103 \text{ mg CO}_2 \text{ m}^{-2} \text{ d}^{-1}$  (Table 4).

### 3.4 Diel flux variations

The fine temporal resolution of the EC technique enables analysis of the diel variations in  $\text{CH}_4$  fluxes from the reservoir surface, which were rather pronounced over Lake Klöntal (Fig. 5b). The median reservoir fluxes determined for each hour of the day yielded a maximum that remained rather constant at  $2.9 \pm 0.1 \text{ mg CH}_4 \text{ m}^{-2} \text{ d}^{-1}$  during peak daytime (11–16 hours CET)—which was roughly 3 times the typical nighttime  $\text{CH}_4$  efflux observed ( $0.9 \pm 0.2 \text{ mg CH}_4 \text{ m}^{-2} \text{ d}^{-1}$ , 23–07 hours CET). During peak daytime, more than 75% of the eddy covariance flux measurements indicated a  $\text{CH}_4$  efflux from the lake, whereas at night ef-

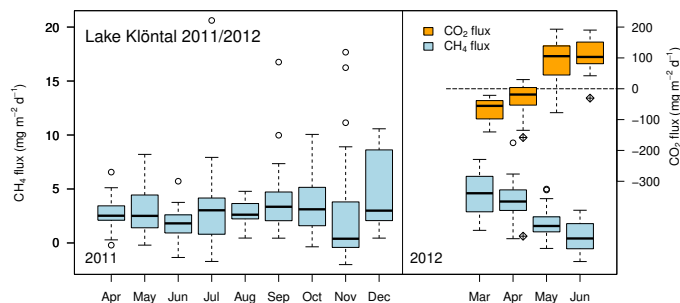


**Fig. 10** Seasonal variability of  $\text{CH}_4$  and  $\text{CO}_2$  fluxes ( $\text{mg m}^{-2} \text{d}^{-1}$ ) in 2011 ( $\text{CH}_4$  measurements only) and 2012 measured by the EC system. Boxes, whiskers and dots show the inter-quartile range (IQR), the data range up to 1.5 times the IQR, and outlier values, respectively. The EC system was installed during the ice-free period, from 13 April until 6 December 2011, and from 29 March 2012 until 22 June 2012.

**Table 2** Annual  $\text{CH}_4$  emission estimate from Lake Klöntal based on eddy covariance flux measurements in 2011 and 2012 near the deepest spot of the reservoir. For January and February 2012 with ice cover we assumed an efflux (numbers in italics) of 23% the average magnitude measured under ice free conditions following Wik et al.<sup>15</sup>.

Lake Klöntal 2011/2012			Methane flux densities			Methane emissions		
Eddy Covariance			[ $\text{mg CH}_4 \text{m}^{-2} \text{d}^{-1}$ ]			[ $\text{t CH}_4 \text{yr}^{-1}$ ]		
Month	Year	Days	Median	Lower	Upper	Total	Lower	Upper
Mar	2012	3	4.6	1.6	7.6	5.6	2.0	9.2
Apr	2011	18	2.5	2.0	3.0	3.1	2.5	3.7
Apr	2012	29	3.8	3.3	4.4	4.7	4.0	5.3
May	2011	31	2.5	1.6	3.4	3.1	2.0	4.1
May	2012	22	1.6	1.1	2.0	1.9	1.3	2.5
<b>Spring</b>			<b>3.0</b>	<b>1.9</b>	<b>4.1</b>	<b>3.7</b>	<b>2.4</b>	<b>5.0</b>
Jun	2011	30	1.8	1.3	2.3	2.2	1.6	2.8
Jun	2012	22	0.4	-0.4	1.2	0.5	-0.4	1.5
Jul	2011	31	3.0	2.1	4.0	3.7	2.5	4.8
Aug	2011	31	2.6	2.2	3.0	3.2	2.7	3.7
<b>Summer</b>			<b>2.0</b>	<b>1.3</b>	<b>2.6</b>	<b>2.4</b>	<b>1.6</b>	<b>3.2</b>
Sep	2011	30	3.4	2.6	4.1	4.1	3.1	5.0
Oct	2011	31	3.1	2.1	4.1	3.8	2.6	5.0
Nov	2011	30	0.4	-0.8	1.6	0.5	-1.0	2.0
<b>Autumn</b>			<b>2.3</b>	<b>1.3</b>	<b>3.3</b>	<b>2.7</b>	<b>1.6</b>	<b>3.8</b>
Dec	2011	6	3.0	-1.2	7.2	3.6	-1.5	8.8
Jan	(ice cover)		<i>0.6</i>	<i>0.5</i>	<i>0.9</i>	<i>0.7</i>	<i>0.6</i>	<i>1.1</i>
Feb	(ice cover)		<i>0.6</i>	<i>0.5</i>	<i>0.9</i>	<i>0.7</i>	<i>0.6</i>	<i>1.1</i>
<b>Winter</b>			<b>1.4</b>	<b>-0.1</b>	<b>3.0</b>	<b>1.7</b>	<b>-0.1</b>	<b>3.7</b>
<b>Annual average</b>			<b>2.2</b>	<b>1.1</b>	<b>3.3</b>	<b>2.6</b>	<b>1.4</b>	<b>3.9</b>

flux dropped to between 50 and 75% of the observed fluxes.

$\text{CO}_2$  fluxes (2012 only, Fig. 5d) were also highest during the day, but not primarily during peak daytime ( $46 \pm 10 \text{ mg CO}_2 \text{ m}^{-2} \text{ d}^{-1}$ ) as for  $\text{CH}_4$ . Rather, peak  $\text{CO}_2$  fluxes occurred at the end of the day when the sun set below the mountains and left Lake Klöntal in full shadow prior to nightfall (hourly median  $144 \text{ mg CO}_2 \text{ m}^{-2} \text{ d}^{-1}$  at 18 hours). The corresponding time period in the morning, before the sun reached the valley bottom, was a short period of negative  $\text{CO}_2$  fluxes (i.e., net  $\text{CO}_2$  uptake), while nocturnal fluxes were basically zero ( $1 \pm 20 \text{ mg CO}_2 \text{ m}^{-2} \text{ d}^{-1}$ ). Both minimum and maximum hourly median  $\text{CO}_2$  fluxes occurred shortly before the clear transition of atmospheric  $\text{CO}_2$  concentrations from night to day (i.e., high to low concentrations) and day to night (i.e., low to high concentrations), respectively (Fig. 5d). Ultimately, the diel course of  $\text{CO}_2$  concentration showed the inverse of  $\text{CH}_4$  concentrations.

The diel cycles of concentrations and fluxes of both gases were tightly linked to horizontal wind speed (Fig. 5e). Its diel pattern was very distinctive and reflects the narrowly channeled flow in a deeply incised mountain valley where only the diurnal up-valley wind typically exceeds  $1 \text{ m s}^{-1}$ , whereas nocturnal winds are rather calm in the range of  $1 \text{ m s}^{-1}$ . Thus, the typical daytime wind system is not along the valley but across the valley (from the southeast; see Fig. 4a), which is easily explained by the steepness of the topography that allows the sun to heat up the southern rock face and produce updrafts that mix the air above Lake Klöntal in a vortices roll along the lake. This means that eddy covariance flux measurements during the day should be closely related to conditions measured at locality X7 (Fig. 1) where the deepest spot of the lake bathymetry is found.

Methane fluxes increased exponentially with wind speed  $U_{10}$  up to  $\approx 3 \text{ m s}^{-1}$ , above which the flux remained relatively constant—although with considerable scatter—at around  $5.24 \text{ mg CH}_4 \text{ m}^{-2} \text{ d}^{-1}$  (Fig. 11). At low wind speeds (i.e., below  $0.67 \text{ m s}^{-1}$ ),  $\text{CH}_4$  fluxes also remained constant at around  $0.8 \text{ mg CH}_4 \text{ m}^{-2} \text{ d}^{-1}$ . In the transition range between  $0.67$  and  $3 \text{ m s}^{-1}$ , the best estimate of  $\text{CH}_4$  fluxes relative to wind speed was  $F_{\text{CH}_4} = (0.29 \pm 0.07) + U_{10}(1.69 \pm 0.04)$ , with  $U_{10}$  in  $\text{m s}^{-1}$  and  $F_{\text{CH}_4}$  in  $\text{mg CH}_4 \text{ m}^{-2} \text{ d}^{-1}$ .

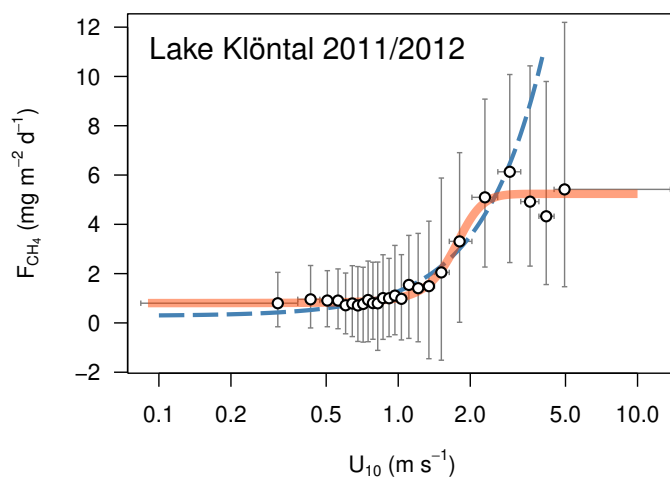


**Fig. 11** Eddy covariance  $\text{CH}_4$  flux as a function of 10-m wind speed  $U_{10}$ . 30-min flux averages were binned in 25 groups of equal number of samples. For each group the median (open circle) and the inter-quartile ranges (horizontal and vertical whiskers) are shown. A power law was fit to median  $U_{10} \leq 3 \text{ m s}^{-1}$  (blue dashed curve,  $F_{\text{CH}_4} = (0.29 \pm 0.07) + U_{10}^{(1.69 \pm 0.04)}$ ). The leveling off at high  $U_{10}$ , however, can only be modeled with a logistic fit (bold orange curve,  $F_{\text{CH}_4} = 0.8 + (4.44 \pm 0.15)/[1 + \exp\{(1.72 \pm 0.06) - U_{10}/(0.24 \pm 0.04)\}]$ ).

Virtual air temperature,  $T_v$ , as measured by the ultrasonic anemometer–thermometer (Fig. 5f), indicated a rather small diel temperature range (DTR), which is characteristic for a local climate with a strong influence from the cool water surface of the reservoir.

### 3.5 Along-lake flux variations

Since the additional sampling locations were not added until August 2011, we could only evaluate the spatial variability in surface  $\text{CH}_4$  from August to November. There was no persistent spa-

tial pattern observed during those months (Fig. 6), but rather a subgrouping of locations could be made based on dissolved CH<sub>4</sub> concentrations. Similarities in concentrations in the western locations (X1–X4), which were nearer the shallow inlet of the reservoir, differed from concentrations in the eastern locations (X5–X7) closer to the outlet and deepest parts of the lake. At the western sites, where shallower depths translated into a large gradient in lake bottom water temperatures ( $T_{LB}$ ) throughout the year (6.4 to 18.6°C), a strong relationship between CH<sub>4</sub> effluxes and  $T_{LB}$  was observed ( $F_{CH_4} = (0.13 \pm 0.01) T_{LB}$ ,  $r^2 = 0.92$ ,  $p < 0.0001$ ; Fig. 9a). In the eastern part of the reservoir, a relationship between  $T_{LB}$  and  $F_{CH_4}$  was also observed, although the more limited monthly  $T_{LB}$  range (4.7 to 8.6°C) resulted in a slightly weaker relationship ( $F_{CH_4} = (0.25 \pm 0.04) T_{LB}$ ,  $r^2 = 0.74$ ,  $p < 0.0001$ ). Note that in both cases the regression intercept was insignificantly different from zero ( $p=0.37$ ) and thus the regression was forced through the origin.

### 3.6 Annual CH<sub>4</sub> emissions from Lake Klöntal and its global warming potential

Annual CH<sub>4</sub> emissions and their uncertainties from the entire lake surface as derived via surface samples along the reservoir and from EC measurements are shown in Tables 3 and 2, respectively. Several assumptions were made to calculate these values, however, and will be discussed in detail below. First, potential losses off-site, such as degassing during pipeline passage, were not included in our estimates. Second, both surface sample-derived and EC based annual estimates suffered from a lack of direct winter emission estimates. Unlike natural lakes in frozen regions, ice covers on Alpine hydropower storages are not safe enough to walk on or deploy instruments because of the substantial vertical displacement of water level below the ice during hydroelectric production. Thus, we assumed 23% of the average CH<sub>4</sub> emissions from months that we could survey, the percentage found by Wik et al.<sup>15</sup>. In this way we assume that CH<sub>4</sub> supersaturation accumulates under the ice which then leads to increased fluxes after the ice has disappeared. This assumption was made for December to March (Table 3). As for the EC estimate, the few days with measurements in December 2011 and March 2012 were considered the best estimates for these two months, so that a reduced flux only had to be assumed for January and February 2012 (Table 2).

Finally, for the surface sample-derived estimate, flux data from each sampling location representing an entire month were weighted according to the surface area of the segment that they represent using equation (7). In the case when a location was not measured, the average flux of the measured locations obtained on that date was used in the weighted average. Ultimately, the annual CH<sub>4</sub> emissions from the lake were estimated at 2.6 (range 1.4 to 3.9) t CH<sub>4</sub> yr<sup>-1</sup> and 1.8 (range 0.5 to 7.4) t CH<sub>4</sub> yr<sup>-1</sup> with the EC (Table 2) and the gas-sampling approaches (Table 3), respectively.

Because CO<sub>2</sub> was not of interest at the beginning of the study, more assumptions had to be made to obtain a realistic annual CO<sub>2</sub> emission estimate: July–October were assumed to produce CO<sub>2</sub> emissions of the same magnitude as measured during June.

**Table 3** Annual CH<sub>4</sub> emission estimate from Lake Klöntal based on monthly gas sampling surveys in 2011 (locations X1–X7, see Fig. 1). Bold numbers are the best estimates for seasonal and annual averages. Number in italics show estimated fluxes (see text for details).

Lake Klöntal	Methane flux densities			Methane emissions		
	[mg CH <sub>4</sub> m <sup>-2</sup> d <sup>-1</sup> ]			[t CH <sub>4</sub> yr <sup>-1</sup> ]		
<b>2011</b>						
Gas Sampling	Mean	Min	Max	Total	Min	Max
Mar	<i>0.5</i>	<i>0.4</i>	<i>0.8</i>	<i>0.6</i>	<i>0.5</i>	<i>0.9</i>
Apr	3.5	0.9	9.8	3.3	0.9	9.1
May	0.9	0.5	1.5	1.0	0.6	1.7
<b>Spring</b>	<b>2.2</b>	<b>0.4</b>	<b>9.8</b>	<b>1.6</b>	<b>0.5</b>	<b>9.1</b>
Jun	3.3	0.9	9.1	1.5	0.9	2.4
Jul	1.0	0.6	1.7	4.9	1.5	13.3
Aug	2.8	2.7	8.8	3.2	0.9	9.6
<b>Summer</b>	<b>2.3</b>	<b>0.6</b>	<b>9.1</b>	<b>3.2</b>	<b>0.9</b>	<b>13.3</b>
Sep	2.3	0.2	5.8	2.5	0.2	6.4
Oct	1.6	0.4	3.2	1.8	0.5	3.5
Nov	1.2	0.1	4.3	1.4	0.1	5.0
<b>Autumn</b>	<b>1.7</b>	<b>0.1</b>	<b>5.8</b>	<b>1.9</b>	<b>0.1</b>	<b>6.4</b>
Dec	<i>0.5</i>	<i>0.4</i>	<i>0.8</i>	<i>0.6</i>	<i>0.5</i>	<i>0.9</i>
Jan	<i>0.5</i>	<i>0.4</i>	<i>0.8</i>	<i>0.6</i>	<i>0.5</i>	<i>0.9</i>
Feb	<i>0.5</i>	<i>0.4</i>	<i>0.8</i>	<i>0.6</i>	<i>0.5</i>	<i>0.9</i>
<b>Winter</b>	<b>0.5</b>	<b>0.4</b>	<b>0.6</b>	<b>0.6</b>	<b>0.5</b>	<b>0.9</b>
<b>Annual average</b>	<b>1.7</b>	<b>0.4</b>	<b>6.3</b>	<b>1.8</b>	<b>0.5</b>	<b>7.4</b>

In contrast to CH<sub>4</sub> there was a net CO<sub>2</sub> uptake measured when the surface water was cold in March and April, hence we assumed that November and December may yield similar uptake rates as April and March, respectively. With these assumptions an annual CO<sub>2</sub> emission of 53 t CO<sub>2</sub> yr<sup>-1</sup> was obtained (Table 4).

**Table 4** Net CO<sub>2</sub> fluxes from Lake Klöntal, March–June 2012, and estimate for annual total CO<sub>2</sub> emissions. Numbers in italics denote estimates without direct measurements (see text for details).

Lake Klöntal 2012			CO <sub>2</sub> flux densities			CO <sub>2</sub> emissions		
Eddy Covariance			[mg CO <sub>2</sub> m <sup>-2</sup> d <sup>-1</sup> ]			[t CO <sub>2</sub> yr <sup>-1</sup> ]		
MONTH	YEAR	Days	Median	Lower	Upper	Total	Lower	Upper
Mar	2012	3	-56	-110	-1	-68	-133	-2
Apr	2012	29	-19	-35	-2	-23	-43	-2
May	2012	22	106	74	137	129	90	167
<b>Spring</b>			<b>10</b>	<b>-24</b>	<b>45</b>	<b>13</b>	<b>-29</b>	<b>54</b>
Jun	2012	22	103	79	127	125	97	154
Jul						130	100	159
Aug						125	97	154
<b>Summer</b>			<b>103</b>	<b>79</b>	<b>127</b>	<b>127</b>	<b>98</b>	<b>156</b>
Sep						125	97	154
Oct						125	97	154
Nov						-23	-43	-2
<b>Autumn</b>						<b>76</b>	<b>50</b>	<b>102</b>
Dec						-68	-133	-2
Jan	(ice cover)					30	21	39
Feb	(ice cover)					30	21	39
<b>Winter</b>						<b>-3</b>	<b>-30</b>	<b>25</b>
<b>Annual average</b>			<b>57</b>	<b>28</b>	<b>86</b>	<b>53</b>	<b>22</b>	<b>84</b>

To address the carbon footprint associated with hydropower generation, we normalized our emission results by electrical energy produced, which amounts to 114 GWh yr<sup>-1</sup>. To allow for a comparison with other hydropower reservoirs, a factor of 34<sup>4</sup> was used to convert CH<sub>4</sub> emissions to CO<sub>2</sub>-equivalents (CO<sub>2,eq</sub>). Our surface sample-derived estimates suggest a carbon cost of 0.54 (range 0.15–2.2) kg CO<sub>2,eq</sub> associated with each MWh of electri-

505 cal energy produced. If EC flux estimates are used as a basis, this number is considerably higher (0.78 (range 0.42–1.16) kg CO<sub>2,eq</sub> MWh<sup>-1</sup>). An additional ≈0.46 kg CO<sub>2</sub> MWh<sup>-1</sup> is expected from the CO<sub>2</sub> emissions (Table 4). With only four months of CO<sub>2</sub> fluxes (Fig. 10, Table 4) an annual estimate is more difficult to obtain than that for CH<sub>4</sub>, but a CO<sub>2</sub> estimate is provided because measured CH<sub>4</sub> fluxes were substantially lower than expected.

## 4 Discussion

### 4.1 Diel cycles of CH<sub>4</sub> and CO<sub>2</sub> fluxes

515 CH<sub>4</sub> fluxes—at least at night—are rather small compared to other reservoirs<sup>14,19</sup>, or lakes<sup>20</sup>, and within the detection limit for EC flux measurements, hence the random scatter around zero which also includes apparent negative fluxes.

On short time-scales the diel cycles of CH<sub>4</sub> and CO<sub>2</sub> fluxes provide some additional insights into the processes leading to GHG emissions. CH<sub>4</sub> fluxes (Fig. 5a) are almost a factor 3 larger during the daytime hours than during the night. This is in agreement with the diel cycle of horizontal wind speed  $U_{10}$  (Fig. 5e) that shows almost calm conditions at night and a pronounced effect of the diurnal up-valley wind system. This affects the piston velocity  $k_{600}$  (Fig. 7) and hence CH<sub>4</sub> efflux. While typical models assume an exponential increase of  $k_{600}$  and thus CH<sub>4</sub> fluxes (as shown in Fig. 11), we observed an upper limit for  $k_{600}$  of  $9.12 \pm 0.37$  cm h<sup>-1</sup> irrespective of wind speeds  $\geq 2$  m s<sup>-1</sup> (Table 1, Fig. 7; midpoint of logistic fit at  $1.70 \pm 0.04$  m s<sup>-1</sup>). The highest wind speeds were observed during a few storms that probably completely mixed the reservoir, thereby exhausting the CH<sub>4</sub> water pool; hence, under high-wind conditions the CH<sub>4</sub> concentration gradient between water and air became the limiting factor for gas efflux, and more turbulent atmospheric mixing no longer increased the CH<sub>4</sub> efflux. This effect is also seen in Figure 11: CH<sub>4</sub> effluxes levelled off around  $5.24$  mg CH<sub>4</sub> m<sup>-2</sup> d<sup>-1</sup> at  $U_{10} > 3$  m s<sup>-1</sup>.

520 The good agreement between the two efforts to estimate annual emissions by taking into account spatial gradients and diel as well as seasonal changes (Tables 3 and 2) is reassuring. In comparison, the EC method offers the advantage of a much richer set of data that can resolve driving factors such as temperature, wind-speed and mixing.

### 4.2 Validation of piston velocity models

545 Our determination of  $k_{600}$  from EC flux measurements in comparison with published models (Fig. 7, Table 1) reveals the general dilemma of how fluxes are estimated from concentration gradients and  $U_{10}$  alone. The selection of a single model can substantially affect flux estimates, and even our approach in which we take the average of various published models (Table 1) would not have led to very robust estimates without the direct EC flux measurements. Our finding that  $k_{600}$  showed an upper limit at high wind speeds may be more generally valid for other lakes and reservoirs with limited CH<sub>4</sub> dissolved in the water body: above a specific  $U_{10}$  threshold (2.0 m s<sup>-1</sup> in the case of Lake Klöntal)—which may depend on local conditions such as lake dimensions and depth, sheltering effect by surrounding topography, and sta-

tistical distribution of wind speeds—a further increase in  $U_{10}$  does not lead to higher CH<sub>4</sub> fluxes because under such conditions it is not the turbulent mixing and transport that limits effluxes, but the resupply of CH<sub>4</sub> to the lake surface.

Although all five models (Table 1) assume an exponential increase even at high wind speeds, the overall effect on our spatially integrated annual flux estimates was not detrimental since  $U_{10}$  very rarely exceeded the threshold above which exponential models would heavily overestimate  $k_{600}$ . It is however also important to note that there is a bit of a mismatch between the monthly data interpolated as in Figure 6 and the high-resolution EC data. On a diel timescale the surface temperature changes and therefore also the solubility, which could not be taken in account in equation (5). In addition, convective mixing will change surface temperature by mixing in cold deeper water, thereby also shifting the oversaturation at the surface. Thus, water concentration measurements at hourly or better intervals would be required to further reduce the uncertainty in  $k_{600}$  derived from EC fluxes in our study.

### 4.3 Estimating the carbon footprint

To evaluate the contribution of this reservoir as an anthropogenic CH<sub>4</sub> source, we compared the spatially integrated monthly CH<sub>4</sub> diffusion rates (Table 3) with the integrated time-series of 2011–2012 EC fluxes measured near position X7 (Table 2). We had to adopt slightly different boundary conditions for the ice-covered period: For the spatial integration we assumed that the flux was low (≈23% the flux under absence of ice<sup>15</sup>) during the period from December to February (Table 3). In reality, the ice cover did not start on the first of December and hence some days in early December 2011 could still be covered with eddy covariance flux measurements. In addition, last few days of March 2012 already allowed the re-installation of the EC system, hence we used the December and March measurements as representative for the whole months and only assumed low fluxes (≈23% the flux under absence of ice<sup>15</sup>) during permanent ice cover in January and February for the annual estimates derived from EC measurements (Table 2).

585 The seasonal integration of EC fluxes yielded an estimated overall CH<sub>4</sub> emission from the Klöntal reservoir of 2.6 t CH<sub>4</sub> yr<sup>-1</sup> (Table 2), of which 27% can be attributed to the warm season (July–September) when the reservoir is filled to its maximum. These losses are due to diffusion alone as no ebullition was detected during our hydroacoustic surveys.

600 The EC fluxes provide a more coarse spatial resolution but a much better temporal coverage of fluxes compared to surface sampling considering measurements were continuously recording at 0.05 s resolution, from which EC-derived CH<sub>4</sub> and CO<sub>2</sub> fluxes were calculated in 30-minute intervals. Aggregated to daily and then monthly fluxes for upscaling, these measurements provide a more robust estimate of the fluxes near position X7. The best estimate for the annual CH<sub>4</sub> emissions from EC flux measurements is 29% higher than the spatially weighted estimate obtained from monthly samplings, and thus outside the range of variability of the spatial sampling. Although the relationship between reser-

615 voir bottom water temperatures and CH<sub>4</sub> flux differs between the shallower western part and the deeper eastern part (Fig. 9a) where the EC measurements were performed, the CH<sub>4</sub> fluxes between the two parts of the lake did not differ significantly (t-test, p=0.624).

We thus used the EC flux measurements for an assessment of the GWP of GHG fluxes from the Lake Klöntal reservoir and included a best annual estimate of concurrent CO<sub>2</sub> fluxes from the first half of 2012 (Table 4). The study of Diem et al.<sup>45</sup> has shown that N<sub>2</sub>O only provides a negligible contribution to GHG emissions in alpine reservoirs.

625 Following conversion to CO<sub>2</sub>-equivalents, we can compare annual Lake Klöntal GHG emissions and the contribution of CH<sub>4</sub> to total emissions to that of other reservoirs. Klöntal emits 88.4 t CO<sub>2,eq</sub> yr<sup>-1</sup> as CH<sub>4</sub>, which is roughly 63% of the total global warming forcing when our best estimate for CO<sub>2</sub> emissions is included in the total (141 t CO<sub>2,eq</sub> yr<sup>-1</sup>). Compared to a meta-analysis from global reservoirs<sup>3</sup>, the relevance of CO<sub>2</sub> effluxes from Lake Klöntal (≈37%) was higher than expected. Deemer et al.<sup>3</sup> estimated the average breakdown of GHG contribution to be 79% from CH<sub>4</sub> and 18% from CO<sub>2</sub>, but note their dataset was dominated by low altitude reservoirs and may not be representative of Alpine reservoirs. In addition, reservoirs with active CH<sub>4</sub> ebullition significantly increased the contribution of that GHG to the average carbon emissions in the Deemer et al.<sup>3</sup> synthesis.

630 In a multi-reservoir study on other Alpine hydropower plants across Switzerland, Diem et al.<sup>45</sup> found even lower CH<sub>4</sub> emission rates than those measured in our study. The reservoirs from that study that provide the best comparison with Lake Klöntal (L. Sihl and L. Lungern) emitted only 6–10% of the CH<sub>4</sub> emissions observed from Lake Klöntal. Perhaps the better spatiotemporal resolution and use of EC measurements improved CH<sub>4</sub> estimates in our study as we would not necessarily expect an order of magnitude difference between Alpine reservoirs of similar altitudes. Regardless, this Lake Klöntal study and that of Diem et al.<sup>45</sup> suggest that high altitude, seasonally frozen reservoirs do not likely contribute substantially to global anthropogenic GHG emission budgets, at least not in the form of CH<sub>4</sub>. Diem et al.<sup>45</sup> found that CO<sub>2</sub> dominated carbon emissions from those Alpine reservoirs (up to 99%), while Demarty et al.<sup>46</sup> found the same in three boreal reservoirs. Demarty et al.<sup>46</sup> suggested that seasonal exposure of shallow reservoir sediments to the atmosphere could limit CH<sub>4</sub> production and prevent the CH<sub>4</sub> buildup in sediment porewaters necessary to fuel ebullition, which is the pathway that significantly enhances overall CH<sub>4</sub> emissions. Together these studies suggest that measurements of CO<sub>2</sub> fluxes from boreal and high Alpine reservoirs are necessary in combination with CH<sub>4</sub> in order to accurately estimate carbon footprints. At the same time, measurement techniques or sampling strategies that provide higher spatiotemporal resolution of CH<sub>4</sub> fluxes may find that CH<sub>4</sub> emissions from such reservoirs are higher than expected, as was the case for Lake Klöntal.

665 GHG emission normalized by mean annual electricity production of the Klöntal hydropower scheme (114 GWh yr<sup>-1</sup>) indicated that 1.24 kg CO<sub>2,eq</sub> MWh<sup>-1</sup> are produced from this Alpine reservoir, which is more than one order of magnitude smaller than the

25 kg CO<sub>2,eq</sub> MWh<sup>-1</sup> for the run-of-the-river hydropower scheme of Lake Wohlen on the Swiss plateau (T. DelSontro, pers. comm.) or the 36 kg CO<sub>2,eq</sub> MWh<sup>-1</sup> reported as the upper range of tropical reservoirs by Demarty and Bastien<sup>47</sup>, and far below the range of 10–550 kg CO<sub>2,eq</sub> MWh<sup>-1</sup> for some high-emission reservoirs in tropical regions of Brazil<sup>48</sup>.

670 As an upper limit for GHG emissions, a recent review proposed an average carbon footprint of 980 kg CO<sub>2,eq</sub> MWh<sup>-1</sup> for coal-fired power plants<sup>49</sup>. Lower average GHG emissions of renewable electricity systems have been documented in a recent meta-analysis as 34 and 50 kg CO<sub>2,eq</sub> MWh<sup>-1</sup> for wind energy and solar photovoltaics, respectively<sup>50</sup>. Depending on the boundary conditions, plausible estimates span two orders of magnitude. The operation of a power plant alone is responsible for 23.9% and 13.0% of the carbon footprint of wind energy and solar photovoltaics, respectively<sup>50</sup>, which is 8.1 and 6.5 kg CO<sub>2,eq</sub> MWh<sup>-1</sup> that can be compared with our estimates.

680 The situation is similar in the case of hydroelectricity: The existence and operation of a hydropower reservoir alters the CH<sub>4</sub> and CO<sub>2</sub> fluxes, and thus hydroelectricity is not perfectly carbon neutral relative to the conditions that would have prevailed had the dam never been built<sup>51,52</sup>.

690 Low nutrient inputs and changing water levels might contribute to the rather small observed emissions of Lake Klöntal. Apart from two campgrounds, there are no major settlements in the partially forested catchment area of the lake and therefore nutrient inputs remain low. Reactive phosphate concentrations in the river<sup>53</sup> downstream of Lake Klöntal are consistently below 5 mg P m<sup>-3</sup>. Therefore, the lake is oligotrophic with very high recreational water quality as assessed by local authorities<sup>53</sup>. Low productivity correlates with low methane emissions according to a recent meta-analysis<sup>3</sup>. In addition, large water level fluctuations aerate the littoral sediments during winter months and block methane production close to the sediment surface. Finally, we might have missed additional emission pathways in our study because it was not possible to monitor the period of drawdown during harsh snow and ice in winter. Decreasing water levels could theoretically trigger ebullition<sup>54</sup> and freshly exposed sediment surfaces during drawdown could release methane at significant rates<sup>55</sup>.

## 5 Conclusions

710 Hydropower electricity is a renewable energy source that is valued positively in the context of climate change mitigation as compared to fossil fuel-based electricity generation. Our best estimate for the Lake Klöntal reservoir as derived from EC flux measurements during 2011 and 2012 suggests that average CH<sub>4</sub> and CO<sub>2</sub> emissions are on the order of 2.2 (range 1.1 to 3.3) mg CH<sub>4</sub> m<sup>-2</sup> d<sup>-1</sup> (Table 2) and 57 (range 28 to 86) mg CO<sub>2</sub> m<sup>-2</sup> d<sup>-1</sup> (Table 4). For the entire lake, converted to CO<sub>2</sub>-equivalents, the GHG emissions (from CH<sub>4</sub> and CO<sub>2</sub>) associated with the electrical power generation of 114 GWh yr<sup>-1</sup> was on the order of 1.24 kg CO<sub>2,eq</sub> MWh<sup>-1</sup>, of which 63% could be attributed to CH<sub>4</sub> emissions. The best estimate of CH<sub>4</sub> emissions derived from area-weighted surface water concentration measurements in 2011 yielded a carbon footprint of electricity of 0.54 kg CO<sub>2,eq</sub> MWh<sup>-1</sup> from CH<sub>4</sub>,

roughly 31% less than the EC-derived estimate of 0.78 kg CO<sub>2,eq</sub> MWh<sup>-1</sup>. Both estimates indicate that electricity from the Lake Klöntal reservoir produces a non-negligible carbon footprint and thus contributes to climate change; however, the effect per energy unit is rather small compared to warmer reservoirs at lower elevations and the majority of the reservoirs in the tropical climate zone. It's carbon footprint is roughly 15–20% that associated with the operation of wind energy and solar photovoltaic plants.

**Conflicts of interest:** There are no conflicts of interest to declare

## Acknowledgments

This study was funded by Eawag and ETH Zurich. W.E. acknowledges funding received from ETH Zurich scientific equipment grants 0-43350-07 and 0-43683-11 for components of the EC flux instrumentation. We thank Christian Capello, Kurt Steiner, Bruno Steiger and Urs Beitela from the energy Axpo group who helped us with the logistics and coordination. Additional acknowledgments go to Christian Dinkel and Michael Schurter for technical support and Gijs Nobbe for lab assistance. We also thank Ines Bamberger, Sandro Brunner, Sandra Ogorka, Clío Sideri and Chrysanthi Tsimitri for fieldwork assistance. We are grateful for the technical support provided by Peter Plüss and Thomas Baur.

**Data availability:** Data collected by the authors are made available via doi:10.3929/ethz-b-000169083

## References

- 1 C. Bratrich, B. Truffer, K. Jorde, J. Markard, W. Meier, A. Peter, M. Schneider and B. Wehrli, *River Research and Application*, 2004, **20**, 865–882.
- 2 V. L. St. Louis, C. A. Kelly, E. Duchemin, J. W. M. Rudd and D. M. Rosenberg, *BioScience*, 2000, **50**, 766–775.
- 3 B. R. Deemer, J. A. Harrison, S. Li, J. J. Beaulieu, T. DelSontro, N. Barros, J. Bezerra-Neto, S. M. Powers, M. A. Dos Santos and J. A. Vonk, *Bioscience*, 2016, **66**, 949–964.
- 4 G. Myhre, D. Shindell, F.-M. Bréon, W. Collins, J. Fuglested, J. Huang, D. Koch, J.-F. Lamarque, D. Lee, B. Mendoza, T. Nakajima, A. Robock, G. Stephens, T. Takemura and H. Zhang, in *Anthropogenic and Natural Radiative Forcing*, ed. T. F. Stocker, D. Qin, G.-K. Plattner, M. Tignor, S. K. Allen, J. Boschung, A. Nauels, Y. Xia, V. Bex and P. M. Midgley, Cambridge University Press, Cambridge, United Kingdom and New York, NY, USA, 2013, pp. 129–234.
- 5 D. F. McGinnis, J. Greinert, Y. Artemov, S. E. Beaubien and A. Wüest, *J. Geophys. Res. Oceans*, 2006, **111**, C09007.
- 6 T. DelSontro, D. F. McGinnis, B. Wehrli and I. Ostrovsky, *Environmental Science and Technology*, 2015, **49**, 1268–1276.
- 7 B. Bastviken, J. J. Cole, M. L. Pace and M. C. V. de Bogert, *J. Geophys. Res. Biogeosciences*, 2008, **113**, G02024.
- 8 E. Durisch-Kaiser, M. Schmid, F. Peeters, R. Kipfer, C. Dinkel, T. Diem, C. J. Schubert and B. Wehrli, *J. Geophys. Res. Biogeosciences*, 2011, **116**, G02022.
- 9 K. Oswald, J. Milucka, A. Brand, S. Littmann, B. Wehrli, M. M. M. Kuypers and C. J. Schubert, *PLoS ONE*, 2015, **10**, e0132574.
- 10 D. Bastviken, L. J. Tranvik, J. A. Downing, P. M. Crill and A. Enrich-Prast, *Science*, 2011, **331**, 50.
- 11 L. J. Tranvik, J. A. Downing, J. B. Cotner, S. A. Loiselle, R. G. Striegl, T. J. Ballatore, P. Dillon, K. Finlay, K. Fortino, L. B. Knoll, P. L. Kortelainen, T. Kuster, S. Larsen, I. Laurion, D. M. Leech, S. L. McCallister, D. M. McKnight, J. M. Melack, E. Overholt, J. A. Porter, Y. Prairie, W. H. Renwick, F. Roland, B. S. Sherman, D. W. Schindler, S. Sobek, A. Tremblay, M. J. Vanni, A. M. Verschoor, E. van Wachenfeldt and G. A. Weyhenmeyer, *Limnol. Oceanogr.*, 2009, **54**, 2298–2314.
- 12 C. Zarfl, A. E. Lumsdon, J. Berlekamp, L. Tydecks and K. Tockner, *Aquat. Sci.*, 2015, **77**, 161–170.
- 13 D. Bastviken, J. Cole, M. Pace and L. Tranvik, *Global Biogeochemical Cycles*, 2004, **18**, 1–12.
- 14 T. DelSontro, D. F. McGinnis, S. Sobek, I. Ostrovsky and B. Wehrli, *Environmental Science and Technology*, 2010, **44**, 2419–2425.
- 15 M. Wik, R. K. Varner, K. W. Anthony, S. MacIntyre and D. Bastviken, *Nature Geoscience*, 2016, **9**, 99–105.
- 16 I. Ostrovsky, D. F. McGinnis, L. Lapidus and W. Eckert, *Limnol. Oceanogr.: Methods*, 2008, **6**, 105–118.
- 17 D. Martinez and M. A. Anderson, *Science of the Total Environment*, 2013, **454–455**, 457–465.
- 18 T. DelSontro, M. J. Kunz, T. Kempter, A. Wüest, B. Wehrli and D. B. Senn, *Environmental Science and Technology*, 2011, **45**, 9866–9873.
- 19 W. Eugster, T. DelSontro and S. Sobek, *Biogeosciences*, 2011, **8**, 2815–2831.
- 20 C. J. Schubert, T. Diem and W. Eugster, *Environmental Science and Technology*, 2012, **46**, 4515–4522.
- 21 T. Vesala, W. Eugster and A. Ojala, in *Eddy covariance measurements over lakes*, ed. M. Aubinet, T. Vesala and D. Papale, Springer, Dordrecht Heidelberg London New York, 2012, ch. 15, pp. 365–376.
- 22 M. Jammet, P. Crill, S. Dengel and T. Friborg, *J. Geophys. Res. Biogeosciences*, 2015, **120**, 2289–2305.
- 23 E. Podgrajsek, E. Sahlée, D. Bastviken, S. Natchimuthu, N. Kljun, H. E. Chmiel, L. Klemetsson and A. Rutgersson, *Limnol. Oceanogr.*, 2015, **61**, S41–S50.
- 24 C. M. Poindexter, D. D. Baldocchi, J. H. Matthes, S. H. Knox and E. A. Variano, *Geophys. Research Letters*, 2016, **43**, 6276–6284.
- 25 S. Juutinen, M. Rantakari, P. Kortelainen, J. T. Huttunen, T. Larmola, J. Alm, J. Silvola and P. J. Martikainen, *Biogeosciences*, 2009, **6**, 209–223.
- 26 C. J. Schubert, F. S. Lucas, E. Durisch-Kaiser, R. Stierli, T. Diem, O. Scheidegger, F. Vazquez and B. Müller, *Aquat. Sci.*, 2010, **72**, 455–466.
- 27 W. Eugster and P. Plüss, *Agric. Forest Meteorol.*, 2010, **150**, 841–851.
- 28 E. K. Webb, G. I. Pearman and R. Leuning, *Quart. J. R. Met. Soc.*, 1980, **106**, 85–100.
- 29 M. Mauder, T. Foken, R. Clement, J. A. Elbers, W. Eugster, T. Grünwald, B. Heusinkveld and O. Kolle, *Biogeosciences*,

- 2008, **5**, 451–462.
- 30 T. Foken, R. Leuning, S. R. Oncley, M. Mauder and M. Aubinet, in *Corrections and Data Quality Control*, ed. M. Aubinet, T. Vesala and D. Papale, Springer, Dordrecht Heidelberg London New York, 2012, ch. 4, pp. 85–131.
- 31 W. Eugster, G. Kling, T. Jonas, J. P. McFadden, A. Wüest, S. MacIntyre and F. S. Chapin, III, *J. Geophys. Res.*, 2003, **108**, 4362–4380.
- 32 N. Kljun, P. Calanca, M. W. Rotach and H. P. Schmid, *Boundary-Layer Meteorol.*, 2004, **112**, 503–523.
- 33 S. MacIntyre, R. Wanninkhof and J. P. Chanton, in *Trace Gas Exchange across the Air–Water Interface in Freshwater and Coastal Marine Environments*, ed. P. A. Matson and R. C. Harriss, Blackwell Science, Oxford, 1995, pp. 52–97.
- 34 D. A. Wiesenburg and N. L. Guinasso, *Journal of Chemical & Engineering Data*, 1979, **24**, 356–360.
- 35 P. Ciais, C. L. Sabine, G. Bala, L. Bopp, V. Brovkin, J. G. Canadell, A. Chhabra, R. DeFries, J. Galloway, M. Heimann, C. Jones, C. L. Quéré, R. B. Myneni, S. Piao and P. Thornton, in *Carbon and other biogeochemical cycles*, ed. T. F. Stocker, D. Qin, G.-K. Plattner, M. Tignor, S. K. Allen, J. Boschung, A. Nauels, Y. Xia, V. Bex and P. M. Midgley, Cambridge University Press, Cambridge, United Kingdom and New York, NY, USA, 2013, pp. 465–568.
- 36 J. J. Cole and N. F. Caraco, *Limnol. Oceanogr.*, 1998, **43**, 647–656.
- 37 J. Crusius and R. Wanninkhof, *Limnol. Oceanogr.*, 2003, **48**, 1010–1017.
- 38 S. MacIntyre, A. Jonsson, M. Jansson, J. Aberg, D. E. Turney and S. D. Miller, *Geophys. Research Letters*, 2010, **37**, L24604.
- 39 T. Frost and R. C. Upstill-Goddard, *Limnol. Oceanogr.*, 2002, **47**, 1165–1174.
- 40 F. Guérin, G. Abril, D. Serça, C. Delon, S. Richard, R. Delmas, A. Delmas, A. Tremblay and L. Varfalvy, *J. Marine Systems*, 2007, **66**, 161–172.
- 41 T. DelSontro, K. K. Perez, S. Sollberger and B. Wehrli, *Limnol. Oceanogr.*, 2016, **61**, S188–S203.
- 42 R. Wanninkhof, *Limnol. Oceanogr.: Methods*, 2014, **12**, 351–362.
- 43 B. Jähne, G. Heinz and W. Dietrich, *J. Geophys. Res. Oceans*, 1987, **92**, 10767–10776.
- 44 G. H. Givens and J. A. Hoeting, *Computational Statistics*, Wiley, 2nd edn, 2013.
- 45 T. Diem, S. Koch, S. Schwarzenbach, B. Wehrli and C. J. Schubert, *Aquat. Sci.*, 2012, **74**, 619–635.
- 46 M. Demarty, J. Bastien and A. Tremblay, *Biogeosciences*, 2011, **8**, 41–53.
- 47 M. Demarty and J. Bastien, *Energy Policy*, 2011, **39**, 4197–4206.
- 48 J. P. Ometto, A. C. P. Cimleris, M. A. dos Santos, L. P. Rosa, D. Abe, J. G. Tundisi, J. L. Stech, N. Barros and F. Roland, *Energy Policy*, 2013, **58**, 109–116.
- 49 M. Whitaker, G. A. Heath, P. O'Donoghue and M. Vorum, *J. Industrial Ecology*, 2012, **17**, 789–792.
- 50 D. Nugent and B. K. Sovacool, *Energy Policy*, 2014, **65**, 229–244.
- 51 J. A. Harrison, B. R. Deemer, M. K. Birchfield and M. T. O'Malley, *Environmental Science and Technology*, 2017, **51**, 1267–1277.
- 52 G. Abril, F. Guérin, S. Richard, R. Delmas, C. Galy-Lacaux, P. Gosse, A. Tremblay, L. Varfalvy, M. A. Dos Santos and B. Matvienko, *Global Biogeochemical Cycles*, 2005, **19**, GB4007.
- 53 M. Weibel, *Wasserqualität der Linth und des Sernfs 1959–2013*, Canton of Glarus technical report, 2014.
- 54 A. Maeck, H. Hofmann and A. Lorke, *Biogeosciences*, 2014, **11**, 2925–2938.
- 55 K. E. A. Segarra, V. Samarkin, E. King, C. Meile and S. B. Joye, *Biogeochemistry*, 2013, **115**, 349–361.
- 56 *Eddy Covariance – A Practical Guide to Measurement and Data Analysis*, ed. M. Aubinet, T. Vesala and D. Papale, Springer, Dordrecht Heidelberg London New York, 2012.
- 57 *Climate Change 2013: The Physical Science Basis. Contribution of Working Group I to the Fifth Assessment Report of the Intergovernmental Panel on Climate Change*, ed. T. F. Stocker, D. Qin, G.-K. Plattner, M. Tignor, S. K. Allen, J. Boschung, A. Nauels, Y. Xia, V. Bex and P. M. Midgley, Cambridge University Press, Cambridge, United Kingdom and New York, NY, USA, 2013.